# An Investigation of Microinstabilities in a kW Level Self-Field MPD Thruster

D.L. Tilley*, E.Y. Choueiri**, A.J. Kelly†, R.G. Jahn‡
Electric Propulsion & Plasma Dynamics Lab
Princeton University, Princeton, NJ 08544

## Abstract

Theoretical studies indicate that a variety of microscopic and macroscopic plasma instabilities can significantly affect the performance of the MPD thruster, yet experimental evidence for their existence is extremely limited. The primary objective of this research was to provide experimental evidence for the existence of microinstabilities in the MPD thruster operating at a current level below the "onset current". In particular, to experimentally identify as many of those microinstabilities which exist in the MPD thruster, and to determine which of these is the dominant unstable mode, defined as that microinstability which dictates the anomalous transport properties of the plasma. In addition, due to the fact that this study was conducted in the plume of a 20 kW level MPD thruster, a second objective was to investigate whether the device power level is a determinant factor for the existence of these microinstabilities.

By reviewing the characteristics of many microinstabilities, it was concluded that two are expected to persist throughout the MPD thruster: the generalized lower hybrid drift instability (GLHDI) and the electron cyclotron drift instability (ECDI). From the comparison of the peaks in turbulent power spectra to the linear theory of the GLHDI and ECDI, strong experimental evidence for their existence in the plume of the kW thruster was obtained. Additional evidence was provided by the measurement of the phase velocities associated with the naturally occurring plasma fluctuations; these were also observed to be consistent, within experimental error, with the linear theory of the GLHDI and ECDI. Furthermore, experimental evidence was obtained indicating that the GLHDI may be the dominant unstable mode in the majority of the plume region of the MPD thruster.

To investigate the influence of the device power level on the existence of microinstabilities, the plasma properties in the plume of the kW thruster were measured and compared with those in thrusters operating at higher power levels. It was concluded that the device power level should have little influence on the presence of the microinstabilities in the plasma of the MPD thruster. In addition, it was deduced that the observation of the GLHDI and ECDI in the plume of the kW thruster is indicative that these microinstabilities are prominent throughout the interior of all MPD thrusters, operating at all power levels of current interest.

## I. Introduction

The magnetoplasmadynamic (MPD) thruster is a space propulsion device which utilizes the **J×B** force to accelerate a plasma to exhaust velocities useful for various missions in space (10-50 km/sec)[1]. Currently, the MPD thruster is not efficient enough to make it a viable option for missions of current interest[2]. Typical maximum efficiencies are in the 20-40% range, while a minimum of ~60% is required for the MPD thruster to become competitive with chemical and other electric propulsion devices[2]. Recently, Choueiri, et. al.[3] has suggested that microscopic plasma instabilities may be the dominant mechanism for such inefficient operation. This suggestion provided the impetus for this study of microinstabilities in a kW level self-field MPD thruster.

* Graduate Student, Member AIAA, presently at the Phillips Laboratory, Electric Propulsion Group, Edwards AFB, CA.
** Research Associate
† Senior Research Engineer, Member AIAA
‡ Professor, MAE Department, Fellow AIAA

An enormous body of literature is dedicated to the study of instabilities in **J×B** plasmas[4]. Indeed, there exists a fair amount of research on the effect of plasma instabilities on other electromagnetic acceleration devices utilizing **J×B** forces (e.g. the Hall current accelerator[5-7]). While the study of plasma instabilities in Hall current accelerators and other plasma physics apparatus may be helpful to MPD thruster research; they are not strictly applicable, because the plasma properties in the MPD thruster differ significantly from those of other devices. The MPD thruster plasma is relatively dense and collisional, such that the electron Hall parameter ranges from order one to order ten [$\Omega_e/\nu_e$ ~O(1-10)] and the plasma beta can be as high as ~O(10). Typically, large gradients in plasma properties exist inside of the MPD thruster (excluding the sheath regions). Current densities and induced magnetic fields can span many orders of magnitude; up to ~O($10^3$) A/cm$^2$ and ~O(1) kilogauss in MW level devices. The plasma is typically highly ionized, with charged particle number densities in the $10^{13}$-$10^{16}$/cm$^3$ range, and is relatively isothermal: $T_e \sim T_i \sim$O(1) eV. The unique combination of plasma properties in the MPD thruster necessitates its own theoretical and experimental investigation.

Initial work, concerning the effects of plasma instabilities on MPD thruster performance, focussed on the prediction of the onset of various pathological thruster operation modes. Many instabilities have been invoked as the cause of the so-called "onset current limitation"[8,9], above which high frequency terminal voltage fluctuations and excessive thruster erosion are observed. These include microscopic instabilities such as the Buneman, ion acoustic, and electron acoustic instabilities[10,11]; as well as macroscopic instabilities such as the electrothermal instability[12], among others[13-15]. Experimentally, inconclusive attempts have been made to identify the instability associated with the onset current limitation by the examination of the power spectra of both the terminal voltage and light intensity fluctuations[16,17]. In the case of a MPD thruster with an applied axial magnetic field, plasma instabilities have also been proposed as being responsible for the rotating spoke phenomenon[18-20].

Only recently has the research emphasis shifted towards the investigation of the effects of microinstabilities on MPD thrusters operating at a current level below the onset current. Many observations support the view that microinstabilities do significantly affect MPD thruster performance. These include ionization fractions[21] and line radiation[22] levels much larger than what is expected classically, and the measurements of enhanced plasma resistivity[23].

Emphasis is currently being placed on the theoretical identification of the various microinstabilities which may exist in the MPD thruster[3,12,14,15,24-26], and the identification of the dominant unstable mode, defined as that instability which dictates the anomalous transport properties (e.g. resistivity, viscosity, heat conduction) in the plasma of the MPD thruster. Once the dominant unstable mode has been identified, research can be directed towards the stabilization of the mode by suitable design of the thruster, and/or the minimization of the losses associated with the mode by the manipulation of its non-linear effects. In principle, the identity of the dominant unstable mode may depend on the region of the thruster, may change for different thruster operating conditions, and there may be regions where two microinstabilities have significant contributions to the transport properties of the plasma. Presently, it has been inferred that the dominant unstable mode in the MPD thruster is the generalized

lower hybrid drift instability (GLHDI)[27,28]. For the MPD thruster application, this mode has been studied in a more simplified form known as the modified two stream instability[3,12,24-25]. A more general analysis is available in reference 26.

Experimental verification of the existence of plasma instabilities in the MPD thruster plasma is extremely limited. Most notably, by measurement of the linear dispersion relation, Choueiri, et. al.[3] showed that the plasma in the plume of a MW level MPD thruster is indeed unstable to small density disturbances. In addition, recent measurements have provided evidence for the existence of the GLHDI in the same thruster[26].

The work reported here was intended to provide additional experimental data concerning the existence of plasma instabilities in MPD thrusters operating below the onset current. This research had two objectives. First, to experimentally identify as many of those microinstabilities which are active in the MPD thruster, and to determine which of these is the dominant unstable mode. This work was conducted in the plume of a 20 kW level MPD thruster, raising the issue of the applicability of this research to thrusters operating at higher power levels. Consequently, the second objective was to investigate whether the device power level is a determinant factor for the existence of these microinstabilities.

To achieve these objectives, three separate experiments were performed. First, the plasma properties in the kW level MPD thruster plume were characterized using a triple probe and Hall probe. This characterization was used to compare the plasma properties in the plume of the kW level thruster to known properties in higher power level devices, providing insight into the question of whether the power level can influence the conditions necessary for the existence of those microinstabilities active in the MPD thruster. In the second experiment, the triple probe was used to investigate turbulent fluctuations of plasma properties, as a means to identify the presence of various microinstabilities, and the dominant unstable mode. In the last experiment, measurements of the plasma dispersion relation were used to provide further evidence for the identification of the microinstabilities existing in the kW level MPD thruster plume.

## II. A Brief Review of Microinstabilities Which May Exist in the Plasma of the MPD Thruster

Due to the fact that very little experimental evidence for the existence of microinstabilities in the MPD thruster is available, a brief review of the microinstabilities which may theoretically exist in the MPD thruster is presented. In addition, this review also represents a compilation of possible candidates for the dominant unstable mode.

In the MPD thruster, large current densities constitute a major source of free energy to drive an instability. Experimental measurements have shown that the ratio of the electron drift velocity, $U_e$, to the ion thermal velocity, $V_{ti}$, typically ranges from 1 to 100. On this basis, and for the sake of simplicity, it was assumed that only current driven instabilities are important in the MPD thruster. The number of microinstabilities to be considered is further reduced to those driven by a cross-field current, because the current density is always perpendicular to the magnetic field in the self-field MPD thruster.

For reference purposes, before discussing the characteristics of these instabilities, it is useful to describe the geometry of the equilibrium configuration. The equilibrium configuration is the zero-order profile of the plasma properties, about which the linear perturbation analysis is performed. The result of the perturbation analysis is the linear dispersion relation[4,29]. The equilibrium configuration required for this discussion is fairly simple. It is situated in the ion rest frame with the magnetic field in the z-direction, the electron drift velocity in the y-direction, requiring a gradient in magnetic field in the x-direction. In the cylindrical geometry of the MPD thruster, the negative azimuthal direction corresponds to the z-direction of the equilibrium configuration; and the r-z plane of the MPD thruster corresponds to the x-y plane of the equilibrium configuration, with the y-direction aligned with the electron drift velocity relative to the ions. To investigate the temporal stability of the equilibrium configuration, the linear dispersion relation is solved, such that for a given set of plasma parameters and wavevector, $\mathbf{k}$, a complex frequency, $\tilde{\omega} = \omega + i\gamma$, is obtained[4,29]. For this discussion, the wavevector is considered to vary in the y-z plane with $|k| = (k_y^2+k_z^2)^{1/2} = 2\pi/\lambda$, where $\lambda$ is the wavelength. The superscript '*' on $\omega$ and $\mathbf{k}$ correspond to the real frequency and wavevector corresponding to the maximum growth rate, $\gamma>0$, when $\gamma$ is maximized over $\mathbf{k}$ space. The characteristics of $\omega^*$ and $\mathbf{k}^*$ for each instability are required in the interpretation of the experimental results to be presented later.

Listed in table 1 are five well known microinstabilities driven by a cross-field current which may exist in the plasma of the self-field MPD thruster, along with their characteristics at maximum growth and their main condition for existence. Each instability operates near a natural frequency of the plasma, and each has its own effects on the plasma, in terms of anomalous transport. Microinstabilities requiring $T_i>>T_e$ for existence, such as the electron acoustic instability[30], have been eliminated from consideration, along with those microinstabilities which have a growth rate much smaller than the ion residence time in the thruster, e.g. the universal instabilities[4].

The GLHDI[27,28] has been studied extensively in several more simplified forms, such as the modified two stream instability[25,30-32], the lower hybrid drift instability[33-35], the kinetic cross field streaming instability[36,37], and the Farley-Buneman instability[38,39]. The GLHDI can be excited by relatively low drift velocities and always operates near the lower hybrid frequency, $\omega_{LH}$. The magnitude and direction of $\mathbf{k}^*$ can vary significantly depending on the plasma conditions, such as the presence of gradients, collisions, and the value of the electron plasma beta, $\beta_e$ ($\equiv 2\mu_o n_e \kappa T_e/B^2$). The direction of $\mathbf{k}^*$ can be exactly perpendicular to the magnetic field or be such that $k_z^* \sim k_y^*$; while the magnitude of $\mathbf{k}^*$ can be as large as the inverse electron gyroradius ($k^* r_{Le} \approx 1$) or be much smaller ($k^* r_{Le} << 1$). A review of the above instabilities, and their application to the MPD thruster plasma is presented in reference 26.

In the electron reference frame, the electron cyclotron drift instability (ECDI)[40-44] operates at discrete frequencies near the harmonics of the electron cyclotron frequency ($n\Omega_e$, n=1,2,...). The typical unstable wavelength is much shorter than the electron gyroradius ($k^* r_{Le} >> 1$), and is directed essentially perpendicular to the magnetic field, in the direction of the electron drift velocity.

The Buneman instability is normally considered in non-magnetized plasmas or in systems with a field aligned current[29,45]. It can be shown that for $\beta_e << 1$, the linear dispersion relation of a uniform magnetized plasma with a cross-field drift will reduce to the unmagnetized case provided that $k_z$ is sufficiently large[28,46]. In this case, the Buneman instability will operate near the electron plasma frequency (in the electron frame of reference) with wavelengths much smaller than the electron gyroradius (i.e. $k^* r_{Le} >> 1$).

In a magnetized plasma, for $T_e >> T_i$, the ion acoustic instability operates in two regions of wave number space[28,32]: $kr_{Le} << 1$ [30] and $kr_{Le} >> 1$. In the region of $kr_{Le} >> 1$, where significantly higher growth rates exist, the ion acoustic instability behaves as its non-magnetic counterpart with $\omega^* \approx \omega_{pi}$, and $k^* \approx \lambda_d^{-1}$, where $\omega_{pi}$ is the ion plasma frequency and $\lambda_d$ is the electron debye length. The main condition for existence of the ion acoustic instability is that $T_e/T_i >> 1$, although the existence of temperature gradients and non-maxwellian velocity distributions can significantly alter this criterion, as will be discussed later.

| Instability | Main condition for existence | Maximum growth characteristics in the ion rest frame | |
|---|---|---|---|
| Generalized Lower Hybrid Drift Instability (GLHDI) | Can exist for $U_e < V_{ti}$ | $\omega^* \approx \omega_{LH}$ | $k^* \leq r_{Le}^{-1}$ |
| Electron Cyclotron Drift Instability (ECDI) ($\omega^* \equiv n\Omega_e$ in the electron frame) | $U_e > V_{ti}$ | $\omega^* \approx n\Omega_e\left(\frac{U_e}{V_{ti}} - 1\right)^{-1}$ | $k^* \approx n\Omega_e(U_e - V_{ti})^{-1}$ |
| Buneman Instability ($\omega^* \equiv \omega_{pe}$ in the electron frame) | $U_e > V_{te}$ | $\omega^* \approx (m_e/M_i)^{1/3}\omega_{pe}$ | $k^* \approx \omega_{pe}/U_e$ |
| Ion Acoustic Instability ($kr_{Le} \gg 1$) | $T_e \gg T_i$ , $U_e > (\kappa T_e/M_i)^{1/2}$ | $\omega^* \approx \omega_{pi}$ | $k^* \approx \lambda_d^{-1}$ |
| Drift Cyclotron Instability | $\left(\frac{m_e}{M_i}\right)^{1/2} \leq \frac{r_{Li}}{L_x} \leq \left(\frac{m_e}{M_i}\right)^{1/4}$ | $\omega^* \approx n\Omega_i$ | $k^* \approx r_{Le}^{-1}$ |

Table 1: Five microinstabilities known to exist in **J**×**B** plasmas ($\beta_e \lesssim 1$).

The drift cyclotron instability (DCI)[47,48] operates at discrete frequencies near the harmonics of the ion cyclotron frequency ($n\Omega_i$, n=1,2,...). The wavevector, **k***, is directed perpendicular to the magnetic field and has a magnitude satisfying $k^* r_{Le} \approx 1$. The existence of the DCI depends on the gradient of various plasma properties (which create the cross-field current). The gradient scale length of property x, $L_x$ [$\equiv 1/\nabla(\ln x)$], must be sufficiently small to excite the instability; but not too small, for then the DCI will transform into the GLHDI at wavenumbers near $r_{Le}^{-1}$. The DCI may be considered as either the low current or small gradient limit of the GLHDI. Collisions are also known to transform the DCI into the GLHDI, even when the gradient scale length is not sufficiently small to transform the DCI into the GLHDI in the collisionless case[49].

With this review, it is now possible to assess theoretically which of these microinstabilities may or may not exist in the MPD thruster plasma. Of the five instabilities listed in table 1, only the GLHDI and the ECDI have no fundamental restrictions forbidding their existence in the MPD thruster. Experiments in the MPD thruster have shown that the electron drift velocity is only a small fraction of the electron thermal velocity, effectively stabilizing the Buneman instability. Measurements of the ion temperature in the MPD thruster plasma indicate that typically $T_e \lesssim T_i$[50,51], suggesting that ion acoustic waves are also stable. In spite of the isothermal plasma in the MPD thruster, the ion acoustic instability cannot be eliminated from consideration altogether, because the stability criterion is very sensitive to the actual electron and ion velocity distribution functions, and the main condition for its existence ($T_e \gg T_i$) is based on the assumption that the two-temperature Maxwellian description is accurate. In addition, the presence of an electron temperature gradient has also been shown to destabilize ion acoustic waves in isothermal plasmas[52], suggesting that the ion acoustic instability may operate in the cathode region of the MPD thruster. Finally, in typical MPD thruster plasmas, the DCI is expected to be fully transformed into the GLHDI. Gradient scale lengths are generally much smaller than the ion Larmor radius and the ion Hall parameter, which is the ratio of the ion cyclotron frequency to the ion-ion collision frequency is typically much less that unity [typically: $\Omega_i/\nu_{ii} \sim O(10^{-2})$].

Excluding special circumstances, in which the ion acoustic instability is excited, it is anticipated that only two microinstabilities will be present in the MPD thruster plasma: the GLHDI and the ECDI. As stated earlier, past research investigating the effects of these instabilities, indicate that the GLHDI will be the dominant unstable mode in the MPD thruster plasma. Both instabilities are known to cause significant increases in the plasma resistivity[41-43, 53,54], but non-linear analysis have shown that the ECDI is apparently much weaker than the GLHDI[31,41] and the ion acoustic instability[42]. If the ion acoustic instability does exist in the MPD thruster plasma, further theoretical study will be required to predict the identity of the dominant unstable mode.

## III. The Characterization of the kW level MPD Thruster Plume

Knowledge of the relevant plasma properties is essential for any experimental investigation of plasma instabilities. With the measurements of $n_e$, $T_e$, the azimuthal magnetic field, $B_\theta$, and the current density, **J**, it is possible to calculate most of the relevant plasma properties required to investigate the stability of the MPD thruster plasma. In this section, the results of the characterization of the plasma properties in the plume of the kW level MPD thruster are presented. This characterization will also be used in the investigation of the influence of the thruster power level on the existence of various microinstabilities.

All experiments were conducted in the near-field plume of a steady state, 20 kW level MPD thruster; i.e. z/D<1, where z is the axial distance downstream from the exit plane, and D is the exit plane diameter of the thruster. The fact that these experiments were not conducted inside of the thruster did not limit the scope of this investigation; many studies have shown that significant electromagnetic interactions, characteristic of inside of the MPD thruster, can occur in the plume (e.g. reference 55). Moreover, for the investigation of the existence of plasma instabilities, it will be demonstrated later, that the plasma in the plume is quite similar to that inside of the MPD thruster.

The experiments were conducted in the Princeton 30 kW steady state thruster facility[21,56]. The vacuum tank is 1.5 m in diameter, 6.4 m long, pumped by one 1.2 m diffusion pump, backed by a roots blower and a mechanical pump. With this pumping system, the tank pressure during thruster operation was less than $5 \times 10^{-4}$ torr. Probe positioning was achieved by a pendulum arm, powered by a stepper motor, which swept the probes through the plume[57], allowing for the radial profiles of the plasma properties to be obtained. The steady state MPD thruster used in this research is shown schematically in figure 1. The thruster has coaxial geometry, a 2% thorium, 98% tungsten 0.64 cm diameter cathode, a graphite anode insert with an exit diameter of 3.5 cm enclosed in another graphite cylinder 10 cm in diameter. The plumbing and electrical connections, located behind the thruster, are described in reference 56. Typical operating conditions with the propellant argon are: currents from 500-900A, mass flow rates in the 8-13 mg/sec range, and terminal voltages of 20-30V.

A triple probe[58] was employed to measure the electron temperature and electron number density of the plasma. It has the ability to make essentially instantaneous measurements of $T_e$ and $n_e$, allowing for the attainment of an entire radial profile in a single swing of the pendulum arm through the plume. Details of

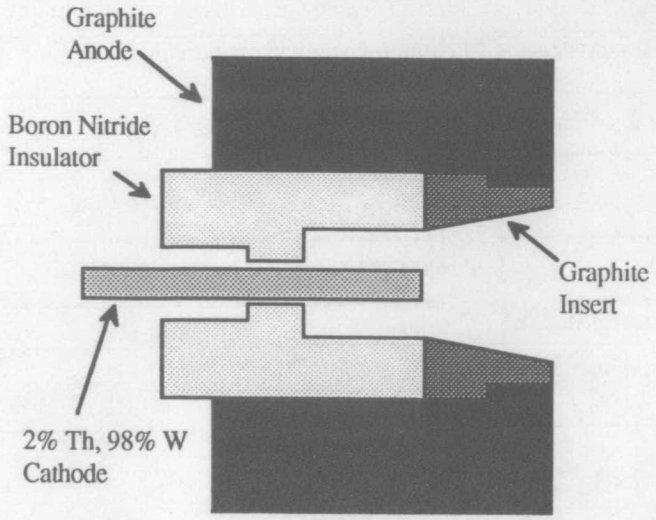


Fig. 1: A reduced-scale schematic of the steady state, 20 kW level MPD thruster.

the apparatus associated with the triple probe are described in reference 57. The triple probe consisted of three cylindrical electrodes configured in a three-in-line fashion (the electrode spacing was 1 mm, the probe radius ($r_p$) was 0.121 mm, and the electrode length was 5 mm). The thin sheath limit criterion, which applies for $r_p/\lambda_d>100$, was not satisfied in the plume of the kW thruster (typically $r_p/\lambda_d$~10-30). Therefore, a modification of the triple probe theory[59], based on the calculations of Laframboise[60], was utilized. Using this theory, $T_e$ and $n_e$ were calculated from the two triple probe outputs: the voltage termed $V_{d2}$ and the current, I. In addition, it was assumed that $T_i=T_e$ and that the ion species were singly ionized. The effect of ions drifting perpendicular to the triple probe, known to significantly affect triple probe performance[59], was accounted for by aligning the triple probe with the ion flow vector as discussed in references 57 and 59. The uncertainty associated with the triple probe measurements was estimated to be ≈10% for $T_e$ and ≈60% for $n_e$, due to unknown ion temperature, unknown species composition, and due to the existence of a non-zero electron drift velocity perpendicular to the probe[59].

In figures 2 and 3, three radial profiles of electron temperature and electron number density in the near-field plume of the kW thruster are shown. The $T_e$ profiles, shown in figure 2, are very similar in shape and magnitude to spectroscopic measurements obtained by Myers[21] at the exit plane of the same thruster. In particular, both indicate a relatively flat profile of $T_e$, except near the centerline. The magnitude of the number density measurements, shown in figure 3, is also consistent with spectroscopic measurements obtained at the exit plane by Myers[21]. The effect of mass flow rate on $T_e$ is small, while $n_e$ is observed to increase slightly with increasing mass flow rate, as observed in other MPD thrusters[61]. Note that the triple probe output was not filtered, indicating that the plasma was not grossly turbulent at these thruster conditions.

Measurements of the azimuthal magnetic field and current density in the plume the kW thruster were obtained by the use of a Hall effect probe[62]. The Hall probe, along with the electronics associated with it, are described in detail in reference 57. It consisted of two Hall generators, displaced axially such that a radial profile of $B\theta$ and $dB\theta/dz$ could be obtained. The axial and radial current densities, used to derive the electron drift velocity with respect to the ions ($U_e=J/n_ee$), were then calculated via Maxwell's equations[63].

Figure 4 shows typical measurements of the azimuthal magnetic field at an axial location of 1.7 cm downstream of the

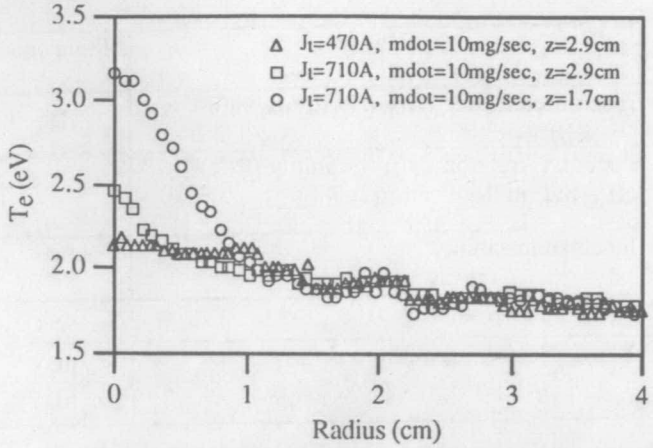


Fig. 2: Typical radial profiles of electron temperature in the near-field plume of the kW level MPD thruster (uncertainty in the measurements was ≈10%).

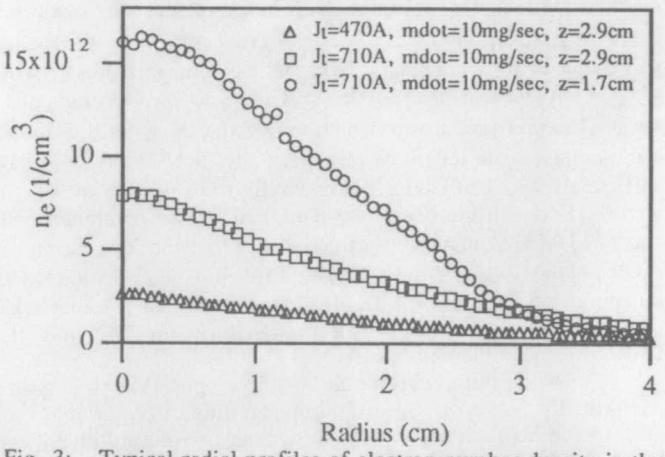


Fig. 3: Typical radial profiles of electron number density in the near-field plume of the kW level MPD thruster (uncertainty in the measurements was ≈60%).

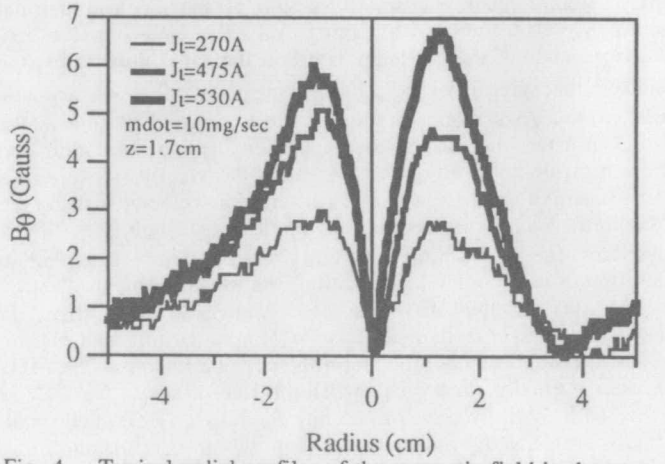


Fig. 4 Typical radial profiles of the magnetic field in the near-field plume of the kW level MPD thruster.

exit plane, at a mass flow rate of 10 mg/sec, as the thruster current is varied. It was observed that the magnetic fields were strongly affected by the thruster current level, while relatively insensitive to mass flow rate variations. The small hump occurring near r=+5 cm, due to mechanical factors, was eliminated in the experiments to be discussed later. Often the magnetic field profiles were asymmetric in shape, due to asymmetries of the plume. Gross asymmetries of the plume creates two problems. First, because the Hall probe was sensitive to $B\theta$ only, the magnitude of **B**, required

to calculate many of the natural frequencies of the plasma, will be underestimated, due to the non-zero $B_r$ and $B_z$ components. Second, the calculation of the axial and radial current densities rely on the symmetry of the plume.

The largest source of error of the magnetic field measurements is due to the uncertainty of the location of the probe ($\Delta r = \pm 0.5$ steps = 1.3 mm). Depending on the region of the plume, the uncertainty in the magnetic field measurement was typically 10-25% and no less than 3%, which was the uncertainty in the calibration. For radii less than 0.75 cm, it is also expected that the probe will significantly perturb the magnetic field by inhibiting the current inducing $B_\theta$[57]. Therefore, in the experiments to be discussed later, only measurements from the r>0.75 cm region of the plume and from reasonably symmetric profiles were considered reliable. Typically, in the region r>0.75, axial current densities ranged from 1 to 10 A/cm$^2$, while maximum radial current densities were in the 1-4 A/cm$^2$ range. Typical uncertainties in these measurements, due to the uncertainty in the position of the probe, were 25-50%.

It should be emphasized that these results, although typical, may not be exactly reproducible. The kW thruster operated in a generally stable manner, such that the results among swings of the pendulum arm were reproducible. But often the results from different test runs were not exactly reproducible, due to the changing geometry of the plume. Consequently, in the experiments discussed later, the plasma properties were measured along with the diagnostics investigating plasma instabilities.

## IV. The Investigation of Turbulent Power Spectra

The rationale behind this experiment stems from the assumption that each microinstability listed in table 1 operates near a different natural frequency of the plasma. By measuring the power spectrum of naturally occurring plasma fluctuations, and comparing it with measured natural frequencies ($f_{ci}$, $f_{LH}$, $f_{ce}$, $f_{pi}$, $f_{pe}$), it is possible to obtain evidence indicating which instabilities are present in the MPD thruster and which instability is the dominant unstable mode. Previous experiments in the MPD thruster[16,17] have investigated the power spectra of the terminal voltage and light intensity measurements without the measurement of the natural plasma frequencies. Furthermore, the terminal voltage and light intensity measurements are integrated over space, which make them extremely difficult to use for the identification of plasma instabilities. This experiment differs from past research in that the frequency content of the local plasma property fluctuations are measured and compared with measurements of the local natural frequencies, allowing for a much clearer interpretation of the spectra.

The triple probe was the primary means by which plasma property fluctuations were measured. The fluctuations of $V_{d2}$ reflect essentially fluctuations of $T_e$ and the electric field component along the electrodes; while fluctuations of the current reflect essentially number density and electron temperature fluctuations[57]. The natural plasma frequencies were obtained by simultaneously sweeping the triple probe and the Hall probe through the plume of the thruster. The triple probe was aligned with the thruster axis; consequently, the uncertainty of the measurements increased because it was no longer aligned with the ion flow vector in all regions of the plume. The uncertainty of the measurements was estimated to be ≈25% for $T_e$, and approximately a factor of two for $n_e$ (i.e. the value of $n_e$ is expected to be within one half to two times the stated value)[59].

The electronics associated with the triple probe are discussed in reference 57. A Nicolet 320 digital oscilloscope, sampling at 5 MHz, recorded the triple probe outputs, resulting in the maximum observable frequency, the Nyquist frequency ($f_N$) of 2.5 MHz. Consistent with the use of low pass filters to minimize aliasing error, the frequency response of the electronic apparatus was tested to be relatively flat up to ~1 MHz. In addition, all power spectra shown in this section have been corrected for the frequency response of the instruments. The frequency response of the triple probe is expected to be flat up to a frequency on the order of the ion plasma frequency (~O(100) MHz)[64], which was well beyond the frequencies investigated (<2.5 MHz). In this experiment, both argon and helium were utilized as propellants.

Three general statements can be made about the measurements taken in the plume of the kW thruster. First, turbulent fluctuations were observed only at high values of $J_t^2/\dot{m}$, the critical value ranged from 40-60 kA$^2$sec/g. Second, the fluctuating amplitudes of $V_{d2}$ and of the current were often observed to be a significant fraction of the mean values. Third, the power spectra of $V_{d2}$ were very similar to that of the current. Furthermore, the power spectrum measurements obtained in this experiment could be placed into two distinct categories: one consistent with the presence of the GLHDI, the other consistent with the presence of both the GLHDI and the ECDI.

Two samples of the first type are shown in figure 5 for argon, and in figure 6 for helium. Plotted is the normalized power spectrum verses frequency, where the normalized power spectrum is equal to $S_{11}(f)/S_{11}(f_m)$, and $f_m$ is the frequency at which the power spectrum, $S_{11}$, is maximum. The scatter in the power spectra, due to the use of discrete Fourier transform techniques, is not physical. The scatter can be reduced by increasing the frequency averaging number, m, which is chosen as a compromise between acceptable statistical scatter and frequency resolution (cf. Appendix A). This type of power spectra, which was prominent throughout the plume region investigated (r≤3 cm, z<D), consisted of a broad band peak at frequencies in the 50 to 200 kHz range, and then fell below the noise level at higher frequencies. Generally, no qualitative difference between spectra obtained in the argon plasma and those from the helium plasma were observed. As will be shown later, the peak in the power spectra is near the Doppler shifted lower hybrid frequency, providing evidence that the GLHDI is present in the kW thruster plume.

Before showing a comparison of the power spectra to the measured natural frequencies, it is useful to discuss where in frequency space the peaks are expected to occur. To assist in the interpretation of the spectra, the linear characteristics of the instabilities are used throughout this section, even though the spectra are turbulent, and non-linear in nature. In fact, only the peaks in the spectra are compared with linear theory; no attempt was made to describe their structure. In the ion rest frame, the frequency at which the power spectrum is maximum is expected to be on the same order of the frequency corresponding to maximum growth (cf. table 1). Due to the fact that the ions are flowing with respect to the triple probe, the peak frequency will be Doppler shifted. The following equation is used to predict the peak frequency in the laboratory frame:

$$f_{lab} = \left| f^* + \frac{\mathbf{k}^* \cdot \mathbf{U_i}}{2\pi} \right| \qquad (1)$$

where | | signifies the absolute value, $\mathbf{U_i}$ the ion flow vector, and $f^*$ and $\mathbf{k}^*$ represent the frequency and wavevector corresponding to maximum growth of the instability in the ion rest frame, which are tabulated in table 1.

For the GLHDI, it is known (cf. section II) that the maximum temporal growth rate, in the ion rest frame, occurs at a frequency near the lower hybrid frequency, but the magnitude and direction of $\mathbf{k}^*$ is extremely sensitive to the plasma properties, and is not known accurately for the plasma conditions of the kW thruster plume. Of particular interest is an estimate of the largest frequency, $f_{max}$, for which the peak in the turbulent spectra is expected to be observed in the laboratory frame. From equation 1, it is seen that the largest value of $f_{lab}$ occurs for the largest value of $k^*$, which corresponds to $k^* r_{Le} \sim 1$ for the GLHDI (cf. table 1). Substituting into equation 1:

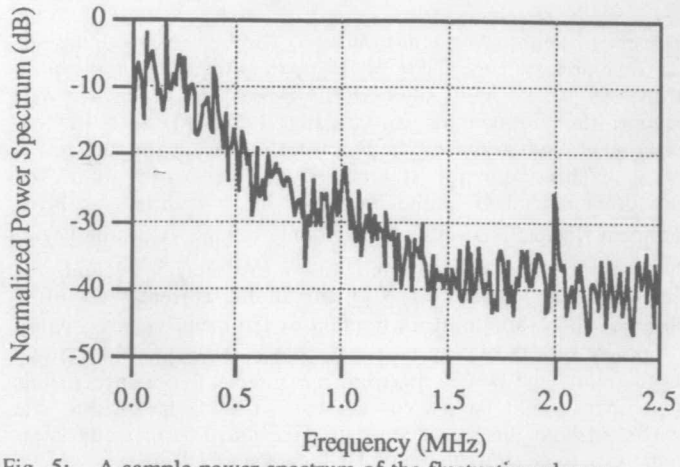


Fig. 5: A sample power spectrum of the fluctuating plasma properties in the plume of the kW level MPD thruster using argon as a propellant (m=4).

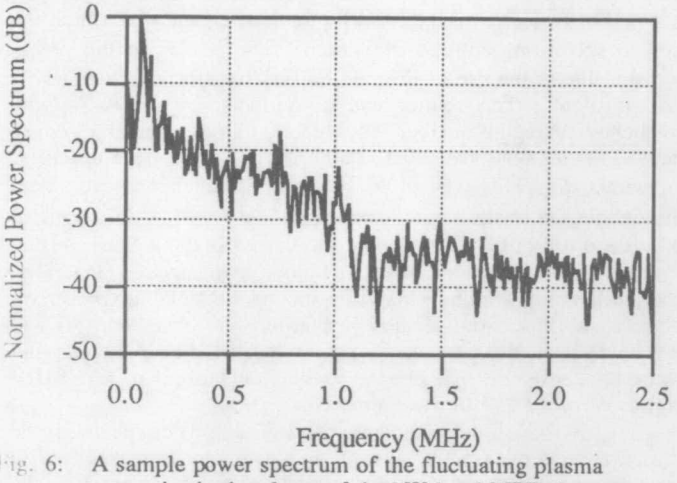


Fig. 6: A sample power spectrum of the fluctuating plasma properties in the plume of the kW level MPD thruster using helium as a propellant (m=4).

$$f_{max} \sim f_{LH} + \frac{U_i}{2\pi r_{Le}} \tag{2}$$

where $r_{Le} = V_{te}/\Omega_e$. The above expression can be written as:

$$\frac{f_{max}}{f_{LH}} \sim 1 + \frac{U_i}{\sqrt{\frac{2\kappa T_e}{M_i}}} \tag{3}$$

The ratio $U_i/(2\kappa T_e/M_i)^{1/2}$ is typically 2-4 in the argon plasma, and ~1 for the helium plasma.

The maximum frequency, $f_{max}$, can be estimated from experimental measurements using the following method: $f_{LH}$ and $r_{Le}$ are computed from the measured magnetic field and $T_e$, and the ion flow velocity is estimated from the following relation[1]:

$$U_i = \frac{\mu_o}{4\pi} \ln\left(\frac{r_a}{r_c}\right) \frac{J_t^2}{\dot{m}} \tag{4}$$

where $r_a$ and $r_c$ are the anode and cathode radius respectively, and $\mu_o$ is the permeability constant. Flow velocity measurements[65] and velocities inferred from thrust measurements[21] in the kW thruster agree fairly well with the above expression (within ~50%).

Plotted in figures 7 and 8 are the normalized power spectra shown in figures 5 and 6 respectively, but with a logarithmic frequency scale. The left most data point, at ≈5 kHz, represents the average power between ~O(100) Hz and ≈10 kHz. Each data point thereafter represents the average power between ±5 kHz of the corresponding frequency. Based on the observation of oscillation-free Hall probe measurements, the power spectra is expected to fall off at frequencies less than on the order of 100 Hz. Indicated on the lower frequency scale are the measured natural frequencies of the plasma (except $f_{pe}$); while along the upper frequency scale, $f_{max}$ associated with the GLHDI and $f_{n=1}$ for the ECDI (to be discussed later) are identified. The plasma properties used to calculate the natural plasma frequencies and the frequencies associated with the identification of the various instabilities in the laboratory frame are tabulated in table 2. The essential feature of these results is the presence of large amplitude, naturally occurring turbulent fluctuations near the lower hybrid frequency (which is different from any of the other natural frequencies by at least two orders of magnitude). These spectra are consistent with the presence of the GLHDI in the plume of the kW thruster.

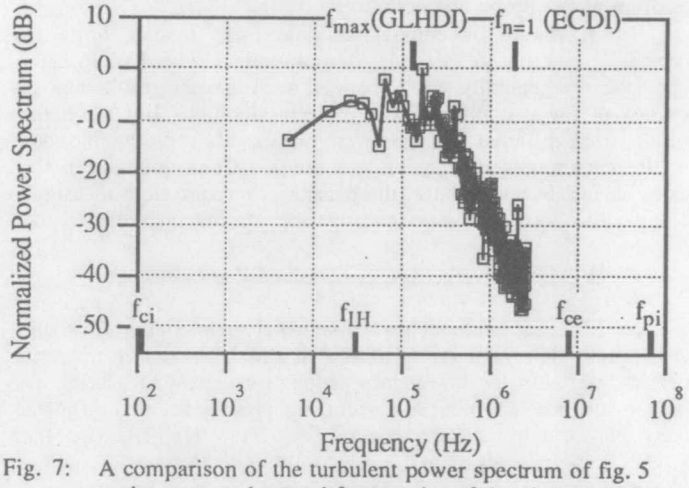


Fig. 7: A comparison of the turbulent power spectrum of fig. 5 to the measured natural frequencies of the plasma, and to the frequencies corresponding to the maximum linear growth rate.

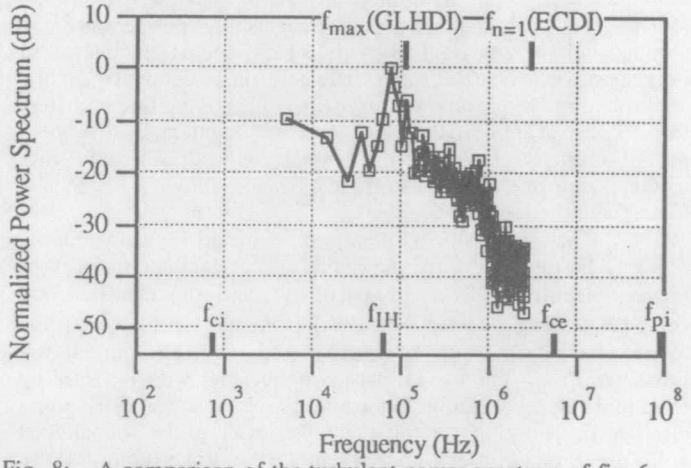


Fig. 8: A comparison of the turbulent power spectrum of fig. 6 to the measured natural frequencies of the plasma, and to the frequencies corresponding to the maximum linear growth rate.

Samples of the second type of power spectra are shown in figures 9 and 10. These spectra consist of the same broad band peak, near the Doppler shifted lower hybrid frequency, but with the inclusion of high power spikes at integral frequencies from each other. These spikes generally occur at much higher frequencies than the Doppler shifted lower hybrid frequency, and are indicative

| Figure | 5,7 | 6,8 | 9 | 10 |
|---|---|---|---|---|
| Propellant | Argon | Helium | Argon | Argon |
| $J_t$ (A) | 685 | 330 | 670 | 600 |
| $\dot{m}$ (mg/sec) | 8 | 1.5 | 10 | 8 |
| Radius (cm) | 1.1 | 1.1 | 2.2 | 0.8 |
| Axial location (cm) | 1.6 | 1.6 | 1.6 | 1.6 |
| $T_e$ (eV) (±20%) | 1.9 | 4.3 | 1.5 | 2.1 |
| $n_e$ (1/cm$^3$) (±x2) | $4.7\times10^{12}$ | $7.3\times10^{11}$ | $2.0\times10^{12}$ | $2.7\times10^{12}$ |
| B (Gauss) | 3.0±0.5 | 2±1 | 5±1 | ~2 |
| $J_r$ (A/cm$^2$) | -0.75±0.25 | $\|J_r\|<0.25$ | -1±0.5 | ~-1 |
| $J_z$ (A/cm$^2$) | -4±1 | $\|J_z\|<0.25$ | +1±0.5 | ~-3 |
| $\beta_e$ † | ~40 | ~30 | ~5 | ~60 |
| Flow angle (deg.)* | ~30 | ~30 | ~40 | ~20 |
| $U_i$ (km/sec)* | ~9.4 | ~11.7 | ~7.2 | ~7.2 |
| $f_{max}$ (GLHDI)† | ~130 kHz | ~120 kHz | ~190 kHz | ~70 kHz |
| $f_{n=1}$ (ECDI)† | ~1.9 MHz | ~3 MHz | ~700 kHz | ~830 kHz |
| $\Delta I/I$ | 0.30 | 0.09 | 0.04 | 0.16 |
| $\Delta V_{d2}/V_{d2}$ | 0.25 | 0.12 | 0.02 | 0.09 |

Table 2: A tabulation of the measured, estimated(*), and calculated(†) plasma parameters corresponding to the turbulent power spectra in figures 5-10.

of the presence of the ECDI in the plume of the kW level MPD thruster. This type of spectra can also be seen in figure 5, with faint peaks at 1 and 2 MHz.

Assuming these spikes are a manifestation of the ECDI, their location in frequency space can be described by the following relation:

$$f_n = \frac{nf_{ce}}{\left(\frac{U_e}{V_{ti}} - 1\right)}\left|\left(1 - \frac{\mathbf{J}}{J}\cdot\frac{\mathbf{U_i}}{V_{ti}}\right)\right| \qquad (n=1, 2, 3...) \qquad (5)$$

where $V_{ti}=(2\kappa T_i/M_i)^{1/2}$. This expression was obtained by substituting $f^*$ and $\mathbf{k}^*$ from table 1 into equation 1, and using the fact that $\mathbf{k}\cdot\mathbf{U_e}>0$ is required for the instability to operate. The frequency, $f_n$, can be predicted from the measurements of B, J, $n_e$, $T_e$, and by assuming that $T_i=T_e$, estimating the direction of $\mathbf{U_i}$ from separate flow angle measurements[57], and by the use of equation 4 to calculate $U_i$. All of these measurements, estimates, and calculations are tabulated in table 2. When $f_{n=1}$ was calculated to be greater than the Nyquist frequency, the high power spikes were not seen, and when it was predicted that $f_{n=1}$ was less than the Nyquist frequency, the location of the spikes were observed to agree with equation 5 within experimental error (which was a factor of 2-3). This evidence suggests that the ECDI is also prominent throughout the near-field plume of the kW thruster ($r\leq3$ cm, $z<D$). In addition, the sharpness of the peaks in frequency space suggest that the measurement of the turbulent power spectra, in conjunction with equation 5, can be used as a check on the measurements of other plasma diagnostics in the MPD thruster.

Finally, it should be stated that no conclusions can be reached about turbulence occurring near the other natural frequencies, because they were not in the viewing range of the experiment. Furthermore, it is not expected that this turbulence, if it exists, will be consistently Doppler shifted into the viewing range. The Doppler shift of the ion cyclotron harmonics is expected to be too small to be seen in this experiment. Typically $k^*$ is much smaller than the inverse electron gyroradius ($k^* << r_{Le}^{-1}$) when the GLHDI is also active[66]. It may also be possible for turbulence occurring at frequencies near $f_{pi}$ and $(m_e/M_i)^{1/3}f_{pe}$ (in the ion rest frame) to be Doppler shifted into the viewing range of the experiment if $\mathbf{k}^*\cdot\mathbf{U_i}<0$. This is not expected to be observed on a regular basis because $f_N << f^*$ and $f_N << |\mathbf{k}^*\cdot\mathbf{U_i}|$.

## V. The Measurement of the Plasma Dispersion Relation

Large amplitude, naturally occurring plasma property fluctuations (i.e. plasma turbulence) are the non-linear, saturated state manifestation of plasma instabilities. For this reason, microinstabilities in the plume of the kW thruster were identified by comparing only the gross features of the turbulent power spectrum with linear stability theory. A more direct approach in the identification of microinstabilities is to measure the linear dispersion relation, along with the plasma properties required by the linear stability model, and compare the experimental results with theory. This approach was the aim of this experiment.

In the plume of the kW thruster, where $\beta_e>>1$, many practical considerations limited the scope of this type of experiment. Currently, no linear theory is available which accounts for all of the physics associated with the high beta region of the MPD thruster[26]. In addition, the accuracy of plasma dispersion relation and plasma property measurements are limited such that a careful comparison of experiment with linear theory would not be fruitful; indeed, the ion temperature and ion flow velocity, required by the model, were not measured at all. The ion temperature was assumed to be approximately equal to $T_e$, and $U_i$ was inferred from equation 4. In light of these limitations, it was desired that the results of this experiment would provide an "order-of-magnitude" type of evidence in support of the presence of the GLHDI and ECDI in the plume of the kW thruster.

The essence of this experiment consists of two Langmuir probes placed a distance $d_{12}$ apart. These probes are biased negative with respect to the plasma potential to measure ion saturation current fluctuations, which are assumed to reflect ion number density fluctuations only. By measuring the phase difference between the fluctuations at each of the probes, the plasma dispersion relation can be derived. In reference 67 it is shown that the wavevector component along the line of the probes, k(f), and the phase velocity, $V_\phi(f)$, as a function of frequency can be obtained from the following relations:

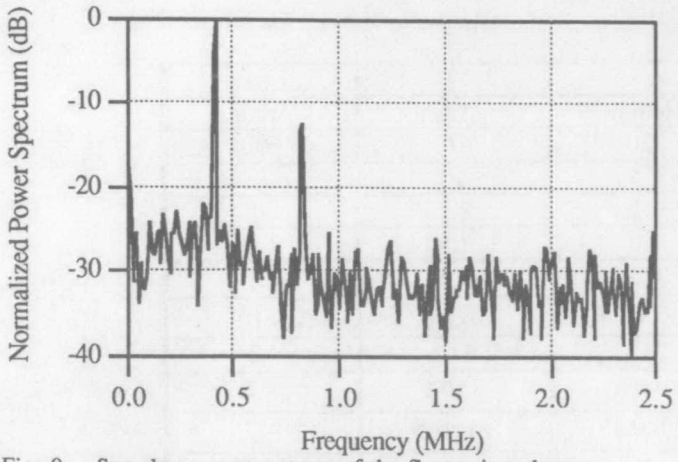


Fig. 9: Sample power spectrum of the fluctuating plasma properties in the plume of the kW level MPD thruster (m=4). This power spectrum is consistent with the presence of the ECDI.

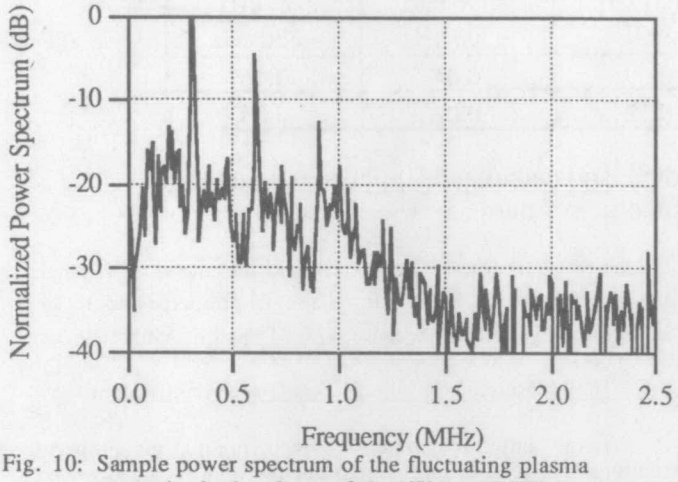


Fig. 10: Sample power spectrum of the fluctuating plasma properties in the plume of the kW level MPD thruster (m=4). This power spectrum is consistent with the presence of the ECDI.

$$k(f)d_{12} = \tan^{-1}\left(\frac{-\mathrm{Im}S_{12}(f)}{\mathrm{Re}S_{12}(f)}\right) \quad (6)$$

$$V_\varphi(f)=\frac{2\pi f}{k(f)} \quad (7)$$

where $\mathrm{Im}S_{12}$ and $\mathrm{Re}S_{12}$ are the real and imaginary parts of the cross spectrum of the two probe signals (cf. Appendix A).

The data, to be presented later, were obtained by passively recording ion saturation current fluctuations, reflecting naturally occurring plasma fluctuations. Technically, a non-linear theory is required to describe the phase information obtained from this experiment; however, it is commonly observed that saturated-state plasma fluctuations still retain much of their linear characteristics[68]. Along with the plasma dispersion relation measurements, radial profiles of the plasma properties were measured by the thruster-axis-aligned triple probe and the Hall probe. In this experiment, only argon was used as a propellant.

Details of the experimental apparatus associated with this experiment is described in reference 57. Two asymmetric double probes, oriented perpendicular to the thruster axis, were used to measure the ion saturation current fluctuations. The two double probes were placed such that the larger electrodes were situated nominally 5 mm apart along the thruster axis, which was the main direction of the electron drift in the kW thruster plume. Across the electrodes of the two probes, a fixed bias (nominally ~20V) insured that the double probes operated in the ion saturation regime, and AC current probes were used to record the ion current fluctuations. Each of these signals was then amplified, filtered (to reduce aliasing error), and recorded on a Nicolet 320 digital oscilloscope sampling at a 2 MHz rate. Phase shifts due to the electronics were measured to be less than five degrees up to 550 kHz.

Measurements were taken at various regions of the plume and under various thruster operating conditions. It was generally observed that the phase velocity was relatively independent of frequency over the frequency range of 100 to 500 kHz ($0.7 \lesssim f/f_{LH} \lesssim 10$), which was the region where the measurements were most accurate. Typically $V_\phi$ ranged from ≈8-15 km/sec for $50 \lesssim J_t^2/\dot{m}[kA^2sec/g] \lesssim 60$, and from ≈20-30 km/sec for $60 \lesssim J_t^2/\dot{m}[kA^2sec/g] \lesssim 90$. The phase velocity was always directed in the +z direction for regions of the plume where $J_z>0$ and $J_z<0$.

A typical phase velocity measurement is shown in figure 11, along with the coherence spectrum (cf. Appendix A) associated with this measurement, in figure 12. At low frequencies, the coherence was very close to unity, indicating the presence of coherent wave phenomenon. The error associated with the phase velocity measurement is due to statistical scatter, aliasing error, and the uncertainty in the phase shift due to the electronics[69]. The large error at low frequencies is due to the large fractional uncertainty of the frequency and phase shift measurement (cf. equation 7), while at high frequencies (>500 kHz), statistical scatter and aliasing error dominate.

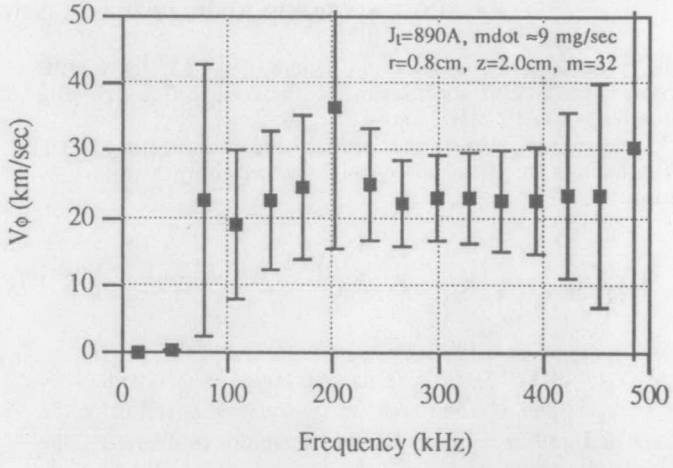


Fig. 11: A typical measurement of the phase velocity ($B\theta$=10±2 Gauss, $T_e$=3.2±20% eV, $n_e$=2.1x10$^{13}$ ±x2/cm$^3$, $J_r$=-3±1 A/cm$^2$, $J_z$=-12±4 A/cm$^2$, $\Delta I/I \approx 0.05$).

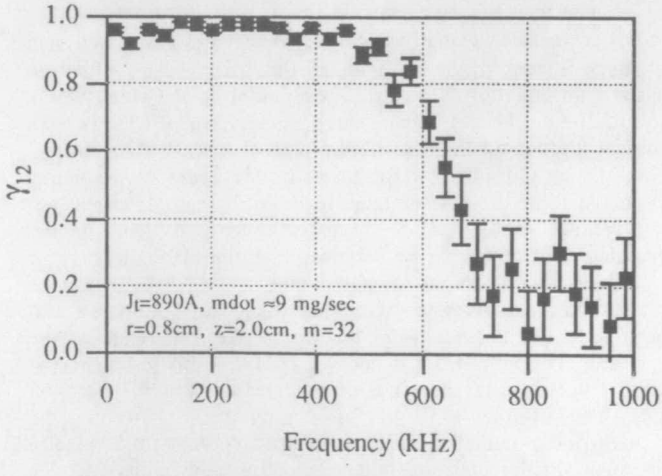


Fig. 12: The coherence spectrum corresponding to fig. 11.

The magnitude of $V_\phi$, and the observation that $V_\phi$ was relatively constant over the frequency range investigated both compare favorably with theoretical expectations. For the high beta region of the MPD thruster, the phase velocities are expected to be greater than, but on the order of, the ion thermal velocity ($V_{ti}=2.2[T_i(eV)]^{1/2}$ km/sec for argon) and relatively independent of frequency (in the ion rest frame)[26,35]. In the laboratory frame, the phase velocity will be increased by an increment $\mathbf{U_i}\cdot\mathbf{k}/|\mathbf{k}|$, which for the data shown in figure 11 is approximately 12 km/sec. Assuming $T_i \sim T_e$, the magnitude of the phase velocity is definitely near the theoretically expected values.

The power spectra of the ion current fluctuations, obtained in this experiment, sometimes exhibited the same high power spikes seen in the experiment of section IV. Furthermore, the location of the spikes in frequency space were observed to agree with equation 5 within experimental error. By investigating the magnitude of $V_\phi$ associated with these spikes, it was possible to gain further evidence for the existence of the ECDI in the plume of the kW thruster.

In theory, the phase velocity associated with each harmonic of the ECDI is very near the ion thermal velocity (in the ion rest frame). In the laboratory frame, the phase velocity is expressed as:

$$V_\phi \equiv V_{ti} + \mathbf{U_i}\cdot\frac{\mathbf{k}}{|\mathbf{k}|} \qquad (8)$$

This expression, which represents the resonance condition between the energy absorbing ions and the negative energy Bernstein harmonics[40], is expected to be very resilient among the different plasma regimes of the MPD thruster. In fact, in its turbulent state, as in this experiment, equation 8 is also expected to be accurate[42].

The measurements of the phase velocity were observed to be consistent with equation 8. Figures 13-15 show a typical example of this type of data. The amplitude of the cross-spectrum is shown in figure 13 to illustrate the presence of the spikes at frequencies of 290 and 580 kHz. In figure 14 it is observed that the coherence associated with these spikes (as noted by the filled circles) is very high. Finally, the phase velocity associated with the spikes are ≈9 km/sec which is near theoretical expectations (assuming $T_i \sim T_e$). The plasma properties were not measured during this test run, but the measurement is illustrative of this type of data. It was consistently observed that $V_\phi \approx 7$-12 km/sec at the frequencies corresponding to the spikes in the power and cross spectra.

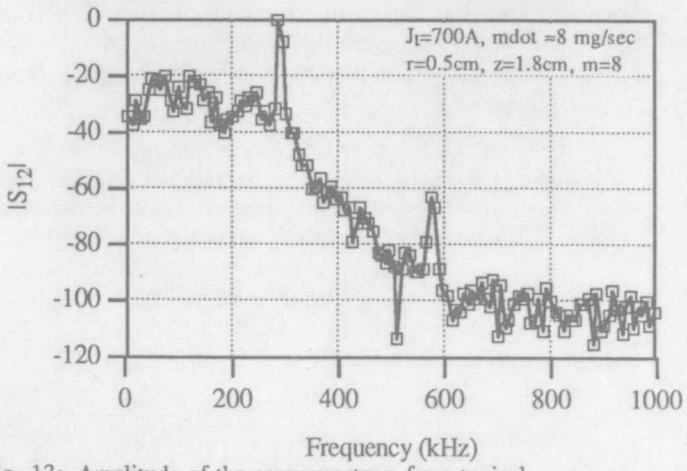


Fig. 13: Amplitude of the cross spectrum for a typical measurement of the phase velocity in the presence of the spikes associated with the ECDI.

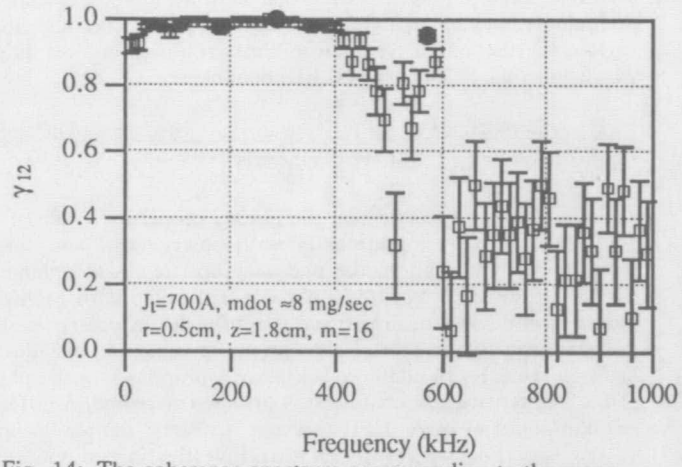


Fig. 14: The coherence spectrum corresponding to the cross spectrum shown in fig. 13. The filled circles correspond to the peaks in the cross spectrum.

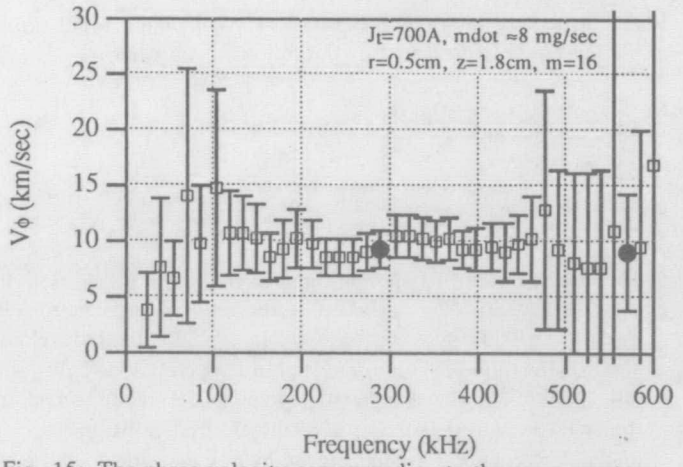


Fig. 15: The phase velocity corresponding to the cross spectrum shown in fig. 13. The filled circles correspond to the peaks in the cross spectrum.

In summary, order of magnitude comparisons of linear theory with phase velocity measurements associated with the naturally occurring plasma fluctuations were consistent with the presence of the GLHDI and ECDI in the plume of the kW level MPD thruster.

## VI. The Identification of the Dominant Unstable Mode

Assuming the broadband peak and the high power spikes in the turbulent power spectra of section IV are manifestations of the GLHDI and ECDI respectively, it may be possible to distinguish which of these instabilities is the dominant unstable mode in the plume of the kW thruster. The basis of this investigation is that the power associated with each of the instabilities is indicative of its effects on the transport properties of the plasma, e.g. the relative strength of the ECDI is assumed to be proportional to the fractional power associated with the high power spikes.

The following statements summarize the observations made in this experiment. For $\Delta I/I$ or $\Delta V_{d2}/V_{d2}$ greater than 0.2 ($\Delta$ represents the root mean square of the fluctuating component), no high power spikes were present in the spectra, or the spikes contributed a negligible fraction of the power. For $\Delta I/I$ or $\Delta V_{d2}/V_{d2}$ less than 0.2, the percentage power associated with the spikes ranged from 0 to 100%. Consistent with theoretical expectations[31,41], these facts indicate that the GLHDI may be the dominant unstable mode in the majority of the plume of the

kW thruster; although, it appears that the effects of the ECDI cannot be ignored when investigating the transport properties of the MPD thruster plasma. Note that these results are considered preliminary; not enough data was collected to distinguish those regions of the plume and those thruster operating conditions where either the ECDI or the GLHDI dominated.

## VII. A Comparison of MPD Thruster Plasmas at Three Different Power Levels

It is well known that the plasma properties inside of the MPD thruster vary significantly with power level and spatial location. In this section, the plasma properties in the plume of the kW level MPD thruster are compared with those of higher power level devices to investigate the influence of power level on the existence of the cross-field current driven microinstabilities listed in table 1. In addition, the plasma properties in the plume of the kW thruster are compared with those measured in different spatial regions of other MPD thrusters, to assess the applicability of the experimental results of this investigation to the inner regions of all MPD thrusters, operating at any power level.

The plasma properties to be compared are those of which that the stability of the plasma depend on. In the ion rest frame, the dispersion relation [$\tilde{\omega}(\mathbf{k})=\omega(\mathbf{k})+i\gamma(\mathbf{k})$] of the MPD thruster plasma can be represented by the following equation:

$$\tilde{\omega}=\tilde{\omega}(k;\frac{U_e}{V_{ti}},\frac{T_i}{T_e},\frac{\omega_{pe}}{\Omega_e},\frac{\nu_e}{\omega_{LH}},\frac{M_i}{m_e},\beta_e,\frac{U_{\nabla B}}{U_e},\frac{U_{\nabla n}}{U_e},\frac{U_{\nabla T}}{U_e},\frac{U_{Rc}}{U_e},\frac{U_{E\times B}}{U_e}) \tag{9}$$

The effects of the first six non-dimensional terms are characterized in reference 26, where $U_e/V_{ti}$ is the ratio of the electron drift velocity, with respect to the ions, to the ion thermal velocity, $T_i/T_e$ is the ratio of the ion to electron temperature, $\omega_{pe}/\Omega_e$ is the ratio of the electron plasma frequency to the electron cyclotron frequency, $\nu_e/\omega_{LH}$ is the ratio of the electron collision frequency to the lower hybrid frequency, $M_i/m_e$ is the ratio of the ion to electron mass, and $\beta_e$ is the electron plasma beta. Note that the ratio of the ion collision frequency to the lower hybrid frequency is not included in equation 9, because this ratio can be related to $\nu_e/\omega_{LH}$ and $M_i/m_e$ when Coulomb collisions dominate, as they do in the MPD thruster. The last five non-dimensional terms characterize the effect of gradients and magnetic field curvature on the stability of the plasma. These terms consist of the ratio of the drift velocity, associated with the gradient of a plasma property or the curvature of the magnetic field, to the actual electron drift velocity, $U_e$. The expressions for each of these drift velocities are shown below[70]:

$$|U_{\nabla B}|=\frac{V_{te}^2}{2\Omega_e}\frac{1}{L_B} \qquad |U_{\nabla n}|=\frac{V_{te}^2}{2\Omega_e}\frac{1}{L_n}$$

$$|U_{\nabla T}|=\frac{V_{te}^2}{2\Omega_e}\frac{1}{L_T} \qquad |U_{Rc}|=\frac{V_{te}^2}{2\Omega_e}\frac{1}{R_c} \tag{10}$$

where:

$$L_B=\frac{1}{\nabla(\ln B)} \qquad L_n=\frac{1}{\nabla(\ln n_e)} \qquad L_T=\frac{1}{\nabla(\ln T_e)} \tag{11}$$

and $R_c$ is the radius of curvature of the magnetic field. $U_{E\times B}/U_e$ characterizes the effect of the E×B drift ($|U_{E\times B}|=E/B$) on the stability of the plasma. The effects of various combinations of the drift velocities have been treated in many studies[26]. In many situations, quite a few of the gradient drift terms can be related to the first six non-dimensional parameters; consequently, all of the non-dimensional parameters in equation 9 may not be independent of each other.

An ideal study of the influence of the power level on the non-dimensional plasma parameters would require the spatial mapping of J, $n_e$, $T_i$, $T_e$, and the plasma potential ($V_p$) throughout a thruster with fixed geometry, fixed $J_t^2/\dot{m}$, at power levels which are many orders of magnitude apart. Although no such investigation exists, and no spatial maps of the ion temperature exist, spatial maps from separate studies in thrusters with nearly the same $J_t^2/\dot{m}$, dimensional scale, and propellant (argon) can be combined as an approximation to this ideal study. The plasma properties of the kW thruster $J_t^2/\dot{m}$=49 $kA^2sec/g$, P=15 kW) will be compared with those of two thrusters operating at higher power levels. The first thruster is that of Tahara, et. al.[71], operating at the following conditions: $J_t^2/\dot{m}$=18 $kA^2sec/g$ and P=370 kW. The plasma of the second thruster was characterized in three separate studies: J and $n_e$ were obtained from reference 72, $T_e$ from reference 73, and $V_p$ in reference 74 for the following operating conditions: $J_t^2/\dot{m}$=52 $kA^2sec/g$ and P=2.7 MW. A comparison of the plasma properties in these three thrusters will represent a power level variation of two orders of magnitude.

Considering the fact that the plasma properties vary significantly with spatial location, inside and outside of the MPD thruster, a many order of magnitude variation of a non-dimensional parameter with power level is assumed to be the minimum requirement for the power level to be a determinant factor on whether any of the cross-field current driven microinstabilities may or may not exist in the MPD thruster. Then a more detailed examination of this parameter will determine if its large variation will completely extinguish and/or excite any of the instabilities in a particular region of the thruster. In table 3, order-of-magnitude values of the non-dimensional plasma parameters are tabulated for three regions of the MPD thruster: inside of the thruster, inside of the thruster but near the exit plane, and the near-field plume region of the thruster. For the sake of clarity, the centerline region of the thruster has been excluded from table 3, because many of the non-dimensional parameters vary considerably within this region, plus its exclusion is not expected to change any of the conclusions that will be discussed later. Assuming that the order of magnitude of $T_i/T_e$ is not affected by thruster power level, and by comparing the order of the non-dimensional parameters, in each of the three regions, no strong trend with power level can be identified. Therefore, it is concluded that the device power level is not a determinant factor for the existence of the cross-field current driven microinstabilities listed in table 1. An example of a more appropriate scaling parameter is $J_t^2/\dot{m}$, which can change much of these parameters significantly.

Table 3 can also be used to investigate the applicability of experiments conducted in the plume to other regions of the thruster. The following non-dimensional parameters are observed to change considerably within the thruster: $\beta_e$, $U_{\nabla B}/U_e$, $U_{\nabla n}/U_e$, and $U_{Rc}/U_e$. $U_{\nabla T}/U_e$ may also change by many orders of magnitude, but $U_{\nabla T}$ is generally small compared to the other drift velocities, due to the existence of relatively small electron temperature gradients in the MPD thruster. It can be shown, using equations 10, 11, and Ampere's law that:

$$\frac{|U_{\nabla B}|_r}{U_{er}}=\frac{\beta_e}{2} \qquad \frac{|U_{\nabla B}+U_{Rc}|_z}{U_{ez}}=\frac{\beta_e}{2}$$

$$\frac{|U_{\nabla n}|_r}{U_{er}}=\frac{L_{Bz}}{L_{nz}}\frac{\beta_e}{2} \qquad \frac{|U_{\nabla n}|_z}{U_{ez}}=\frac{\beta_e}{2L_{nr}\left(\frac{1}{L_{Br}}+\frac{1}{R_c}\right)}$$

| MPD Thruster | Princeton Univ.: Steady State kW level MPD Thruster | Osaka Univ.: MY-I MPD Thruster | | Princeton Univ.: Configuration "A" MPD Thruster | | |
|---|---|---|---|---|---|---|
| Power (kW) | 15 | 370 | | 2700 | | |
| $J_t^2/\dot{m}$ ($kA^2sec/g$) | 49 | 18 | | 52 | | |
| Current (kA) | 0.7 | 5 | | 17.5 | | |
| $\dot{m}$ (g/sec) | 0.01 | 1.37 | | 5.9 | | |
| Property | Near-Field Plume | Inside Of Thruster | Near The Exit Plane | Inside Of Thruster | Near The Exit Plane | Near-Field Plume |
| $U_e/V_{ti}$ | O(1-10) | O(1) | O(1) | O(1-10) | O(1) | O(1) |
| $T_i/T_e$ | ? | ? | ? | ? | O(1)* | O(1)* |
| $\omega_{pe}/\Omega_e$ | $O(10^2\text{-}10^3)$ | $O(10^2\text{-}10^3)$ | $O(10^3)$ | $O(10^2)$ | $O(10^2)$ | $O(10^2\text{-}10^3)$ |
| $\nu_e/\omega_{LH}$ | $O(10^2)$ | $O(10^2)$ | $O(10^2)$ | $O(10^2)$ | $O(10^2\text{-}10^3)$ | $O(10^3)$ |
| $\beta_e$ | O(1-10) | $O(10^{-1}\text{-}1)$ | O(10) | $O(10^{-2}\text{-}10^{-1})$ | $O(10^{-1}\text{-}1)$ | O(1-10) |
| $U_{\nabla B}/U_e$ | O(1-10) | $O(10^{-1}\text{-}1)$ | O(10) | $O(10^{-2}\text{-}10^{-1})$ | $O(10^{-1}\text{-}1)$ | O(1-10) |
| $U_{\nabla n}/U_e$ | O(1-10) | $O(10^{-1}\text{-}1)$ | O(1-10) | $O(10^{-1})$ | $O(10^{-1}\text{-}1)$ | O(1-10) |
| $U_{\nabla T}/U_e$ | $O(10^{-1}\text{-}1)$ | $O(10^{-1}\text{-}1)$ | O(1) | ? | ? | ? |
| $U_{Rc}/U_e$ | O(1-10) | $O(10^{-1}\text{-}1)$ | O(1-10) | $O(10^{-2}\text{-}10^{-1})$ | $O(10^{-1}\text{-}1)$ | O(1-10) |
| $U_{E\times B}/U_e$ | O(1-10)* | O(1-10) | O(1-10) | O(1) | O(1) | O(1-10) |

Table 3: A comparison of plasma properties in three MPD thrusters operating at different power levels. The propellant is argon, i.e. $M_i/m_e$=73500 (* represents an estimated value, and ? an unknown quantity).

$$\frac{|U_{\nabla T}|_r}{U_{er}} = \frac{L_{Bz}}{L_{Tz}}\frac{\beta_e}{2} \qquad \frac{|U_{\nabla T}|_z}{U_{ez}} = \frac{\beta_e}{2L_{Tr}\left(\frac{1}{L_{Br}} + \frac{1}{R_c}\right)} \qquad (12)$$

The effect of the gradient and curvature of the magnetic field can be characterized by $\beta_e$, $U_e/V_{ti}$, and $T_i/T_e$, of which $\beta_e$ varies significantly within the MPD thruster. The effect of the density gradient can be expressed as depending on $\beta_e$, $L_n$, $L_B$, and $R_c$. It is observed in references 71-74, that the ratio of the gradient scale lengths, in both the r and z directions, are relatively constant throughout the thruster. Consequently, the variation of $U_{\nabla n}/U_e$ in the MPD thruster by many orders of magnitude can again be characterized by $\beta_e$. The same reasoning also applies to the ratio of $U_{\nabla T}$ to $U_e$. Therefore, of the non-dimensional parameters listed in equation 9 which vary considerably within the thruster, all are characterized by the variation of $\beta_e$.

The implication of the above conclusions is that for the identification of microinstabilities in the MPD thruster, experiments conducted in the plume of the kW thruster are only applicable to the high $\beta_e$ regions of the MPD thruster operating at any power level. Furthermore, many theoretical investigations[26,35,36,40,44] have shown that increasing $\beta_e$ has the effect of reducing the growth rates of the GLHDI and ECDI, indicating that the near-field plume (or the high $\beta_e$ region) of the MPD thruster is the most difficult region for these instabilities to operate. From the evidence, presented in sections IV and V, indicating that the existence of the GLHDI and ECDI in the plume of the kW thruster, it is inferred that the GLHDI and ECDI are also prevalent throughout the $\beta_e$~O(1) and $\beta_e$<<1 regions inside of the MPD thruster, operating at any power level.

## VIII. Conclusions

The primary objective of this research was to provide experimental support for the existence of microinstabilities in the MPD thruster operating at a current level below the onset current. In particular, to experimentally identify as many of those microinstabilities which exist in the MPD thruster, and to determine which of these is the dominant unstable mode. This research was conducted in the plume of a 20 kW level MPD thruster, raising the question of the applicability of this research to thrusters operating at higher power levels. Consequently, an additional objective of this research was to investigate whether the device power level is a determinant factor for the existence of these microinstabilities.

Due to the lack of experimental evidence, the theoretical characteristics of many of the microinstabilities which may exist in the MPD thruster were reviewed. It was concluded that two current-driven microinstabilities are suspected to persist throughout the MPD thruster: the generalized lower hybrid drift instability (GLHDI) and the electron cyclotron drift instability (ECDI). From the comparison of the peaks in turbulent power spectra to the linear theory of the GLHDI and ECDI, strong experimental evidence for their existence in the kW thruster plume was obtained. Additional evidence was provided by the measurement of the phase velocities associated with the naturally occurring plasma fluctuations, which were also observed to be consistent, within experimental error, with the linear theory of the GLHDI and ECDI.

To investigate the influence of the device power level on the existence of microinstabilities, the plasma properties in the plume of the kW thruster were measured and compared with those in thrusters operating at higher power levels. It was concluded that the device power level should have little influence on the presence of the microinstabilities in the plasma of the MPD thruster. In addition, this comparison of the plasma properties was used to ascertain the applicability of experimental results

obtained in the plume of a MPD thruster to regions inside of the thruster. It was determined that the results of this research are expected to represent the high $\beta_e$ [~O(10)] region of the MPD thruster. Furthermore, due to the stabilizing influence of $\beta_e$, the observation of the GLHDI and the ECDI in the plume of the kW thruster suggests that these instabilities are prevalent throughout the interior of the MPD thruster, operating at any power level.

Finally, it was observed that the largest contributor to the fluctuations of the plasma properties was the broad band peak near the Doppler shifted lower hybrid frequency, indicating that the GLHDI may be the dominant unstable mode in the large $\beta_e$ region of the MPD thruster. This evidence is consistent with theoretical expectations.

The identification of all of the microinstabilities existing in the MPD thruster is essential for the accurate characterization of the transport properties of the plasma. To date, evidence for the existence of the GLHDI and ECDI in the MPD thruster has been obtained. Further investigations, with broader frequency ranges, may identify other modes existing in the MPD thruster, such as the gradient driven ion acoustic instability. In addition, a more systematic mapping of the power spectra inside of the MPD thruster could verify that the GLHDI and ECDI do indeed exist throughout the thruster, and clarify which instability is dominant in the various regions of the thruster. This experimental technique may also be used to identify the instability associated with the onset phenomenon and additional modes existing in an applied field MPD thruster. Finally, the investigation of turbulent power spectra, could be used to investigate the non-linear properties of microinstabilities, such as the identification of their saturation mechanisms[26].

## Acknowledgements

This research is supported, in part, by: NASA Contract No. 954997 and grants from Rocket Research, Inc., the U.S. Department of Energy, Plasma Physics Lab, and G.E. Astro, Space Division, Princeton, NJ.

## Appendix A: The Method of Data Averaging

The uncertainty of quantities derived from discrete Fourier transform techniques are typically dominated by random error. Many averaging techniques exist for the reduction of this error[75], such as the frequency averaging method and the ensemble averaging method. The frequency averaging method was employed in this study, even though both techniques gave comparable results.

Of the 4000 data points obtained by the digital oscilloscope, 2048 were used for data analysis such that a $2^{11}$ data point Fast Fourier transform (FFT) algorithm could be utilized. Before computing the FFT, the time-averaged value of the signal was subtracted from each data point of the oscilloscope trace, and a Hanning window function was applied to the temporal data to reduce leakage effects[76]. At 1024 different frequency bands, the power spectra was calculated using the following expressions:

$$S_{11}(f) = I_1^*(f) I_1(f) \qquad S_{22}(f) = I_2^*(f) I_2(f) \qquad \text{(A1)}$$

where $I_1(f)$ and $I_2(f)$ are the Fourier transform of the measured quantities 1 and 2 and * represents the complex conjugate. To compute the phase difference between the two signals, the cross spectrum is required:

$$S_{12}(f) = I_1^*(f) I_2(f) \qquad \text{(A2)}$$

To reduce statistical scatter, the power spectra and the real and imaginary part of the cross spectra were split into 1024/m subsets in frequency space. In each subset, the power spectra, and the real and imaginary part of the cross spectrum were averaged over the m data points in that subset, and then all of the data points were replaced by the average value at the appropriate frequency.

With a fixed number of data points, the reduction of statistical scatter is traded with the decrease in frequency resolution. When the frequency resolution becomes on the same order of the variation of plasma wave properties in frequency space, an error known as the bias can result (defined as the difference between the actual and calculated mean value of a property)[76]. An illustration of the effect of averaging is shown in reference 69 for data typical of those obtained in these experiments. It was shown that the bias is negligible even for substantial averaging[69]; therefore, the averaging technique had no influence on the spectra other than to reduce data scatter.

In the measurement of phase velocities, a quantity of particular interest in this averaging technique is the coherence spectrum defined below[67,76]:

$$\gamma_{12}^2(f) = \frac{<\mathrm{Re}S_{12}(f)>^2 + <\mathrm{Im}S_{12}(f)>^2}{<S_{11}(f)><S_{22}(f)>} \qquad \text{(A3)}$$

where $< >$ the frequency averaged value. The coherence spectrum characterizes how coherent the signal at probe 1 is to that at probe 2. The coherence ranges from zero to unity; values close to zero corresponding to essentially noise, and values close to unity to the presence of very coherent plasma waves. In addition, the variance of the derived plasma wave properties is a strong function of the coherence; higher $\gamma_{12}$ corresponds to reduced data scatter.

## References

1) Jahn, R.G., The Physics of Electric Propulsion, McGraw Hill, 1968.
2) Sovey, J.S. and Mantenieks, M.A., "Performance and Lifetime Assessment of MPD Arc Thruster Technology", J. Prop. & Power, 7, 1991, p. 71.
3) Choueiri, E.Y., et. al. "Current-Driven Instabilities of an Electromagnetically Accelerated Plasma", IEPC Paper No. 88-042, 1988.
4) Cap, F., Handbook on Plasma Instabilities, Vol. 1&2, Academic Press, NY, 1976 & 1978 respectively.
5) Janes, G.S. and Lowder, R.S., "Anomalous Electron Diffusion and Ion Acceleration in a Low-Density Plasma", Phys. Fluids, 9, 1966, p. 1115.
6) Arefev, V.I., "Plasma Acceleration in Crossed Electric and Magnetic Fields", Sov. Phys. Tech. Phys., 19, 1974, p. 446.
7) Shishkin, G.G. and Gerasimov, V.F., "Plasma Instabilities in Accelerators with Closed Electron Drift", Sov. Phys. Tech. Phys., 20, 1976, p. 1171.
8) Barnett, J.W. and Jahn, R.G., "Onset Phenomena in MPD Thrusters", AIAA Paper No. 85-2038, 1985.
9) Lawless, J.L. and Subramaniam, V.V., "Theory of Onset in Magnetoplasmadynamic Thrusters", J. Prop. & Power, 3, 1987, p. 121.
10) Shubin, A.P., "Dynamic Nature of Critical Regimes in Steady-State High Current Plasma Accelerators", Sov. J. Plasma Phys., 2, 1976, p. 18.
11) Choueiri, E.Y., et. al., "MPD Thruster Plasma Instability Studies", AIAA Paper No. 87-1067, 1987.
12) Niewood, E.H., et. al., "Electrothermal and Modified Two Stream Instability in MPD Thrusters", AIAA No. 90-2607, 1990.
13) Schrade, H.O., et. al., "Stability Problems in Magnetoplasmadynamik ARC Thrusters", AIAA Paper No. 85-1633, 1985.
14) Rempfer, D., et. al., "Investigation of Instabilities in MPD Thruster Flows Using a Linear Dispersion Relation", IEPC Paper No. 88-071, 1988
15) Wagner, H.P., et. al., "Gradient Driven Instabilities in Stationary MPD Thruster Flows", AIAA No. 90-2603, 1990.
16) Kuriki, K. and Iida, H., "Spectrum Analysis of Instabilities in MPD Arcjet", IEPC Paper No. 84-28, 1984.
17) Merke, W.D., et. al., "Nozzle Type MPD Thruster Experimental Investigations", IEPC Paper No. 88-028, 1988.
18) Malliaris, A.C., "Oscillations in an MPD Accelerator", AIAA J., 6, 1968, p. 1575.
19) Hassan, H.A. and Thompson, C.C., "Onset of Instabilities in Coaxial Hall Current Accelerators", AIAA No. 69-230, 1969.
20) Smith, J.M., "Electrothermal Instability - An Explanation of the MPD Arc Thruster Rotating Spoke Phenomenon", AIAA Paper No. 69-231, 1969.
21) Myers, R.M., "Energy Deposition in Low Power Coaxial Plasma Thrusters", Ph.D. Thesis, Princeton University, June

1989. (See also: IEPC Paper No. 88-024, 1988)
22) Abramov, V.A., et. al., "Investigation of Electron Temperature and Plasma Radiation in a Quasi-Stationary High-Current Discharge Between Coaxial Electrodes", in A Survey of Phenomena in Ionized Gases, International Atomic Energy Agency, Vienna, 1968, p. 3.1.11.8.
23) Lovberg, R.H., "Plasma Problems in Electric Propulsion", in Methods of Experimental Physics (Vol. 9): Plasma Physics (Part B), edited by Griem and Lovberg, Academic Press, 1971, Chap. 16, p. 251. (See also: AIAA No. 69-234, 1969)
24) Hastings, D.E. and Niewood, E., "Theory of the Modified Two- Stream Instability in a Magnetoplasmadynamic Thruster", J. Prop. & Power, 7, 1991, p. 258.
25) Choueiri, E.Y., et. al., "Current-Driven Plasma Acceleration Versus Current-Driven Energy Dissipation, Part 1: Wave Stability Theory", AIAA Paper No. 90-2610, 1990.
26) Choueiri, E.Y., "Electron-Ion Streaming Instabilities of an Electromagnetically Accelerated Plasma", Ph.D. Thesis, Princeton University, October 1991.
27) Hsia, J.B., et. al., "Generalized Lower-Hybrid-Drift Instability", Phys. Fluids, 22, 1979, p. 1737.
28) Lemons, D.S. and Gary, S.P., "Current-Driven Instabilities in a Laminar Perpendicular Shock", J. Geophys. Res., 83, No. A4, 1978, p. 1625.
29) Mikhailovskii, A.B., Theory of Plasma Instabilities, Vol. 1 & 2, Consultants Bureau, NY, 1974.
30) Aref'ev, V.I., "Instability of a Current-Carrying Homogeneous Plasma", Sov. Phys. Tech. Phys., 14, 1970, p. 1487.
31) McBride, J.B., et. al., "Theory and Simulation of Turbulent Heating by the Modified Two-Stream Instability", Phys. Fluids, 15, 1972, p. 2367.
32) Lashmore-Davies, C.N. and Martin, T.J., "Electrostatic Instabilities Driven by an Electric Current Perpendicular to a Magnetic Field", Nucl. Fusion, 13, 1973, p. 193.
33) Krall, N.A. and Liewer, P.C., "Low-Frequency Instabilities in Magnetic Pulses", Phys. Rev. A, 4, 1971, p. 2094.
34) Gladd, N.T., "The Lower Hybrid Drift Instability and the Modified Two Stream Instability in High Density Theta Pinch Environments", Plasma Phys., 18, 1976, p. 27.
35) Davidson, R.C., et. al., "Effects of Finite Plasma Beta on the Lower-Hybrid-Drift Instability", Phys. Fluids, 20, 1977, p. 301.
36) Wu, C.S., et. al., "A Kinetic Cross-Field Streaming Instability", Phys. Fluids, 26, 1983, p. 1259.
37) Tsai, S.T., et. al., "Effect of Electron Thermal Anisotropy on the Kinetic Cross-Field Streaming Instability", J. Plasma Phys., 32, Part 1, 1984, p. 159.
38) Lee, K., Kennel, C.F., Kindel, J.M., "High Frequency Hall Current Instability", Radio Sci., 6, 1971, p. 209.
39) Schmidt, M.J. and Gary, S.P., "Density Gradients and the Farley-Buneman Instability", J. Geophys. Res., 78, 1973, p. 8261.
40) Lashmore-Davies, C.N., "Instability in a Perpendicular Collisionless Shock Wave for Arbitrary Ion Temperatures", Phys. Fluids, 14, 1971, p. 1481.
41) Lampe, M., et. al., "Theory and Simulation of the Beam-Cyclotron Instability", Phys. Fluids, 15, 1972, p. 662.
42) Galeev, A.A., et. al., "Anomalous Plasma Resistance Due to Instability at Cyclotron Harmonics", JETP Letters, 15, 1972, p. 294.
43) Aref'ev, V.I. and Chermov, A.A., "Anomalous Resistivity of a Transverse Plasma Current at Electron-Cyclotron Harmonics", Sov. Phys. Tech. Phys., 19, 1975, p. 1522.
44) Zhou, Y.M., et. al., "Stabilizing Effects of a Magnetic Field Gradient in a Perpendicular Shock Wave on Electron Cyclotron Drift Instability", Phys. Fluids, 27, 1984, p. 2049.
45) Buneman, O., "Dissipation of Currents in Ionized Media", Phys. Rev., 115, 1959, p. 503.
46) Gary, S.P., "Longitudinal Waves in a Perpendicular Collisionless Plasma Shock, II. Vlasov Ions", J. Plasma Phys., 4, Part 4, 1970, p. 753.
47) Mikhailovskii, A.B. and Timofeev, A.V., "Theory of Cyclotron Instability in a Non-Uniform Plasma", Sov. Phys.-JETP, 17, 1963, p. 626.
48) Gladd, N.T. and Huba, J.D., "Finite Beta Effects on the Drift-Cyclotron Instability", Phys. Fluids, 22, 1979, p. 911.
49) Huba, J.D. and Ossakow, S.L., "Destruction of Cyclotron Resonance in Weakly Collisional, Inhomogeneous Plasmas", Phys. Fluids, 22, 1979, p. 1349.
50) Bruckner, A.P. and Jahn, R.G., "Exhaust Plume Structure in a Quasi-Steady MPD Accelerator", AIAA J., 12, 1974, p. 1198.
51) Kilfoyle, D.B., et. al., "Spectroscopic Investigation of the Exit Plane of an MPD Thruster", IEPC Paper No. 88-027, 1988.
52) Priest, E.R. and Sanderson, J.J., "Ion Acoustic Instability in Collisionless Shocks", Plasma Phys., 14, 1972, p. 951.
53) Davidson, R.C. and Gladd, N.T., "Anomalous Transport Properties Associated with the Lower-Hybrid-Drift Instability", Phys. Fluids, 18, 1975, p. 1327.
54) Brackbill, J.V., et. al., "Non-Linear Evolution of the Lower Hybrid Drift Instability", Phys. Fluids, 27, 1984, p. 2682.
55) Boyle, M.J., et. al., "Flowfield Characteristics and Performance Limitations of Quasi-Steady Magnetoplasmadynamic Accelerators", AIAA J., 14, 1976, p. 955.
56) Chamberlain, F.R., "Electropositive Surface Layer MPD Cathodes", M.S. Thesis, Princeton University, May 1989.
57) Tilley, D.L., "An Investigation of Micro-instabilities in a kW level Self-Field MPD Thruster", M.S. Thesis, Princeton University, Oct. 1991.
58) Chen, S.L. and Sekiguchi, T., "Instantaneous Direct-Display System of Probe Parameters by Means of Triple Probe", J. Appl. Phys., 36, 1965, p. 2363.
59) Tilley, D.L., et. al., "The Application of the Triple Probe to MPD Thruster Plumes", AIAA Paper No. 90-2667, 1990.
60) Lamframboise, J., "Theory of Cylindrical and Spherical Langmuir Probes in a Collisionless Plasma at Rest", ITIAS Report No. 100, 1966.
61) Maisenhalder, F. and Mayerhofer, W., "Jet-Diagnostics of a Self-Field Accelerator with Langmuir Probes", AIAA J., 12, 1974, p. 1203.
62) Botticher, W., "Measurement of Magnetic Fields in Plasmas", in Plasma Diagnostics, edited by W. Lochte-Holtgreven, John Wiley & Sons, NY, 1968, pp. 617-665.
63) Powers, W.E., "Measurements of the Current Density Distribution in the Exhaust of a MPD Arc Jet", AIAA Paper No. 66-116, 1966.
64) Chen, F.F., "Electric Probes", in Plasma Diagnostic Techniques, edited by R.H. Huddlestone and S.L. Leonard, Academic Press, 1965, pp. 113-200.
65) Diamont, K.D., MAE Report No. 1776.28, 1990, Princeton U.
66) Diamond, et. al., "Suppression of the Drift-Cyclotron Instability by Lower-Hybrid-Drift Turbulence", Phys. Fluids, 25, 1982, p. 2005.
67) Smith, D.E., et. al., "Fast-Fourier-Transform Spectral Analysis Techniques as a Plasma Fluctuation Diagnostic Tool", IEEE Trans. Plasma Sci., PS-2, 1974, p. 261.
68) Ellis, R.F. and Motley, R.W., "Current-Driven Collisional Drift Instability", Phys. Fluids, 17, 1974, p. 582.
69) Tilley, D.L., MAE Report No. 1776.27, 1990, Princeton U.
70) Chen, F.F., Introduction to Plasma Physics and Controlled Fusion, Vol. 1, Plenum Press, New York, 1984.
71) Tahara, H., et. al., "Experimental and Theoretical Researches on Arc Structure in a Self-Field Thruster", AIAA No. 87-1093, 1987.
72) Clark, K.E., et. al., "Quasi-Steady Magnetoplasmadynamic Arc Characteristics", AIAA Paper No. 70-1095, 1970.
73) Turchi, P.J. and Jahn, R.G., "Cathode Region of a Quasi-steady MPD Arcjet", AIAA J., 9, 1971, p. 1372.
74) Oberth, R.C. and Jahn, R.G., "Anode Phenomena in High-Current Accelerators", AIAA J., 10, 1972, p. 86.
75) Wellstead, P.E., "Spectral Analysis", in Digital Signal Processing, edited by N.B. Jones, Peter Peregrinus Ltd, UK, 1982, pp. 139-161.
76) Jenkins, G.M. and Watts, D.G., Spectral Analysis, Holden-Day, San Francisco, 1968.